Broader Application of the Time-SIFT Method: Proof-of-Concept of 3-D-Monitoring Study Cases with Various Spatiotemporal Scales

Denis Feurer, Sean Bemis, Guillaume Coulouma, Hatem Mabrouk, Sylvain Massuel, Romina Vanessa Barbosa, Yoann Thomas, Jérôme Ammann, Fabrice Vinatier

1

Broader application of the Time-SIFT method: proof-of-concept of 3D-monitoring study cases with various spatio-temporal scales

Feurer, D.[1], Bemis, S.[2], Coulouma, G.[1], Mabrouk, H.[3], Massuel, S.[4], Barbosa, R. V.[5], Thomas, Y.[5], Ammann, J.[6] and Vinatier, F.[1]

[1] *LISAH, Univ Montpellier, INRAE, IRD, Institut Agro, Montpellier, France*

[2] *Department of Geosciences, Virginia Tech, Blacksburg, VA, USA*

[3] *INAT, 43 Avenue Charles Nicolle, Tunis 1082, Tunisia*

[4] *G-EAU, AgroParisTech, Cirad, IRD, INRAE, Institut Agro, Univ Montpellier, Montpellier, France*

[5] *UMR 6539 LEMAR, CNRS, UBO, IRD, Ifremer, IUEM Plouzané, France*

[6] *Université de Bretagne Occidentale, CNRS UMR 6538 LGO, IUEM Plouzané, France*

1.1. Introduction

Photography, aerial photography, satellite earth observation, and now the rapidly expanding accessibility of unmanned aerial vehicles (UAV) based remote sensing and smartphones are a rich source of potential image time series that allow the monitoring of a wide range of phenomena across a broad scope of scientific

domains. Some recent advances in remote sensing hence renewed the tools for the monitoring of 3-D change. This is particularly the case for the monitoring of sub-metric 3-D changes such as geomorphic studies, vegetation, or erosion monitoring (e.g., Marcus and Fonstad 2008; Brodu and Lague 2012; Eltner *et al.* 2016). For a long time, studies focusing on these scales relied on topographic ground surveys which are very cumbersome and costly. Terrestrial laser scanner successfully fulfilled for dense topographic data usually acquired from a total station but still has the drawback of being a ground-based technique (occlusions, implementation cost, difficult coverage of large areas). Dense airborne laser scanner allows now to collect such topographic data but the relative novelty of this technique results in a lack of historical depth. Meanwhile, the last decade saw the rapid expansion of methods from the field of computer vision adopted into the earth sciences community (Westoby *et al.* 2012; Fonstad *et al.* 2013; Bemis *et al.* 2014). Structure from Motion (SfM) photogrammetry is now widely used to provide detailed 3-D description of various natural and anthropogenic objects of interest or systems (see for example reviews from Carrivick *et al.* 2016; Eltner *et al.* 2016 or Smith *et al.* 2016). Moreover, Structure from Motion has allowed for extracting new insights from archival aerial imagery (e.g., Verhoeven 2011; Salach 2017; Sevara *et al.* 2017) and hence have access to an unprecedented historical depth for the monitoring of 3-D change. Still, in order to compare data acquired at different epochs, one must ensure that multi-temporal data share a common geometric reference. Co-registration of data of different epochs is indeed - by nature - the prerequisite of diachronic studies. In some experimental designs, permanent reference points can be established to provide common registration points for a multi-temporal study. However, there are a wide range of examinations for which it is not possible to establish reference points prior to imagery collection. For example, study areas with difficult access or environmental sensitivity may preclude the establishment of semi-permanent reference features. Furthermore, a wealth of temporal data already exists in archival imagery where it would be impossible for new studies to establish ground control references prior to imagery collection.

Archival aerial imagery is the most ancient source of multi-temporal Earth observation data, with coherent archives that go back to the early years of the 20th century (Cowley and Stichelbaut; 2012). Methods for processing time series of the Earth's surface were first focused on this kind of data. These methods can differ according to the available data, but even for the most favorable cases - when all the camera calibration and ancillary data is available - one may still need to perform additional co-registration, as described by (Fischer *et al.* 2011). Two main strategies

exist for co-registration of multi-temporal 3-D datasets. One approach relies on *a posteriori* co-registration of the final 3-D models whereas the other approach utilizes a suite of ground control points that can be found in all images. The first category of studies usually requires the user to have available external fine topographic data, such as a lidar-derived topographic dataset. This is the approach used by (Bakker and Lane; 2017), who noticed that the propagation of linear errors could not be limited during the SfM processing and that these errors resulted in spatial differences between the digital elevation model (DEM) of the different epochs. In such cases, authors perform co-registration with an a priori knowledge of stable zones. The "stable zones" approach has also been favorably used for UAV-based studies (e.g., Haas *et al.* 2016). The second category of studies seeks to have or to create a set of ground control points that may be unambiguously found in all images of the multi-temporal dataset. This strategy seems to be the most used in the photogrammetric community, with remarkable recent works that proposed to automatically determine stable linear features (Nagarajan and Schenk 2016), or more recently, automatically derived multi-temporal ground control points (Giordano *et al.* 2018).

Despite the remarkable methods proposed by these previous works, a non-negligible amount of non-image information is needed, either in the form of external data or in the form of photogrammetric expertise, which significantly reduces the potential for a broader use of existing multi-temporal stereoscopic data. In this context, (Feurer and Vinatier 2018a; Feurer and Vinatier 2018b) proposed a new method which allows a user to establish a unique geometric reference shared by all images of a multi-temporal stereoscopic image dataset. This method takes advantage of the invariance properties of feature detection algorithms such as the Scale Invariant Feature Transform (SIFT, Lowe 2004) to automatically link together images of different epochs and is hence called Time-SIFT. The idea of the Time-SIFT method has its roots in the breakthrough that SfM algorithms proposed in photogrammetry, with the provision of dense sets of matched feature points. Indeed, as noticed by several authors (Westoby *et al.* 2012; Fonstad *et al.* 2013), the fact that SfM processing of multi-view stereoscopic imagery relies first and foremost on image information only opens new possibilities in photogrammetric processing. Among these new possibilities, archival aerial imagery was a compelling candidate because the 'classical' photogrammetric workflows require a lot of ancillary data (calibration certificates) in addition to the images themselves, and images with a specific geometric processing if scanned from analogue photography. The study of (Feurer and Vinatier 2018a; 2018b) showed that the Time-SIFT method allowed for

the provision of stackable multi-temporal DEM from almost image information only. Using imagery that contains temporal change to establish a multi-temporal geometric reference seems counterintuitive as one might expect the change captured between epochs to contaminate the registration or reconstruction. Therefore, the Time-SIFT method requires further testing using test cases with a range of spatio-temporal scales. The initial paper (Feurer and Vinatier 2018b) focused on one particular spatio-temporal scale and phenomena, the use of archival aerial imagery to examine prior 3-D changes linked to human activity. The broader suitability of the method for other spatio-temporal scales and other phenomena depends on the ability of the invariance properties of the SIFT-like algorithm to provide consistent results across varied implementations. This possible invariance is expected to result in a trade-off between the spatio-temporal scale of the image data set and the spatio-temporal scale of the studied processes.

In this context, our study aims to check the potential of the Time-SIFT method on varied test cases with different spatio-temporal scales, from the millimeter/minute to the kilometer/decade. The expected success criteria is the ability of the Time-SIFT method to build a complete (with all images and all epochs) and consistent (all data representing the same 3-D scene at the global scale) multi-temporal 3-D block, as well as provide informative 3-D data allowing for the description and characterisation of temporal change associated with the targeted phenomena.

Considering the relatively low effort required by the Time-SIFT method (which at a minimum requires only image data), a significant gain should be expected relatively to other existing methods, either in terms of working and/or processing time, when using ground control points or external registration data is feasible, or in terms of achievable results when these data are not available, which implies that classical methods would not be applicable.

The chapter is divided into two sections. The first section provides a highlight and a detailed description of the Time-SIFT method. The second section is dedicated to the description of five different test cases, presented in five different subsections. The chapter ends with a synthesis of the findings of these different test cases and concluding remarks.

1.2. The Time-SIFT method

1.2.1. General principle

The underlying hypothesis of the Time-SIFT method is that, given an object or a scene, there may always be a space scale or a set of space scales for which different images taken at different times would show similar local features. A direct consequence of this hypothesis is that SIFT-like algorithms may be able to find homologous points in images of the same scene taken at different times, hence enabling the construction of a multi-temporal image block with a single SfM processing of a whole multi-temporal photogrammetric dataset. The immediate effect of processing all images together in a single block is that they share the same unique geometric reference. Hence the co-registration of multi-temporal data is done from the beginning, and only necessitates image information. This limits the need for external registration data such as ground control points. The principle of the proposed method is depicted in Figure 1.

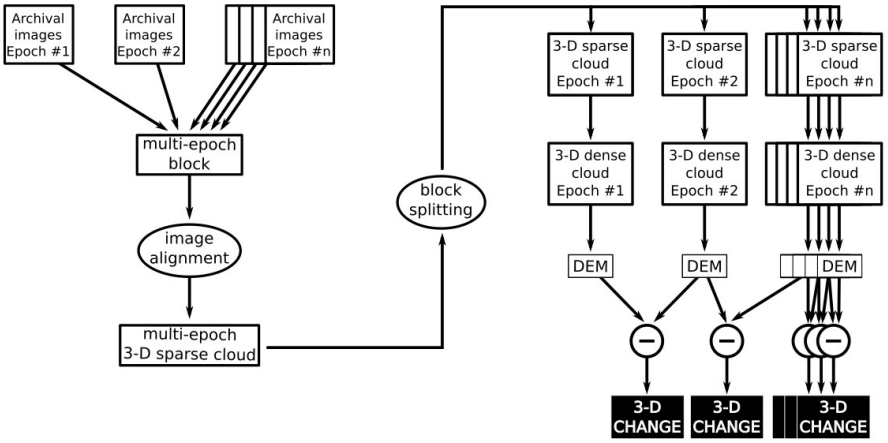

Figure 1. Principle of the Time-SIFT method: use of a single block which joins multi-epoch images in the first step of the Structure from Motion processing. The whole dataset shares the same unique geometry thanks to a single multi-epoch block alignment. Each epoch is then separated while retaining orientation parameters so that subsequent dense 3-D point clouds and Digital Elevation Models (DEM)

maintain the same geometric reference.

The first step of the Time-SIFT method is to construct a single multi-temporal image block (or chunk). In this unique block, all images of all epochs are put together and image orientations are computed simultaneously for the whole dataset. As a result, all image orientations are estimated within only one single geometric reference and different epochs share exactly the same reference system by construction. This drastically simplifies the comparison of the multi-epoch images and may even eliminate the need for co-registration before comparing 3-D models of different epochs.

1.1.2. Existing methods for multi-temporal photogrammetric processing

To the best of our knowledge, with the noticeable and very specific exceptions of (Chanut *et al.* 2017) and (Vargo *et al.* 2017), prior multi-temporal studies utilizing SfM methods calculated 3-D models and image orientation estimates separately between epochs. There are then various strategies to ensure a good co-registration between the dense cloud (or the DEMs) of the different epochs, which can be generalized as two groups. The first group of strategies relies on external data that may be used to register the separate blocks. This usually implies the use of a significant number of Ground Control Points (GCPs). The second group of strategies relies on *a posteriori* co-registration of the different point clouds (or DEMs), either by choosing a reference within the set of points clouds (or DEMs), either by using an external reference point cloud (or DEM) on which all the others are registered. This *a posteriori* registration is needed to tackle the lack of precise positioning data and/or the inaccuracies and error propagation in the photogrammetric processing (e.g. Bakker and Lane 2017). In these classical approaches, each epoch is hence processed separately and an additional step of co-registration is used. The principle of the classical approaches is illustrated on Figure 2 below.

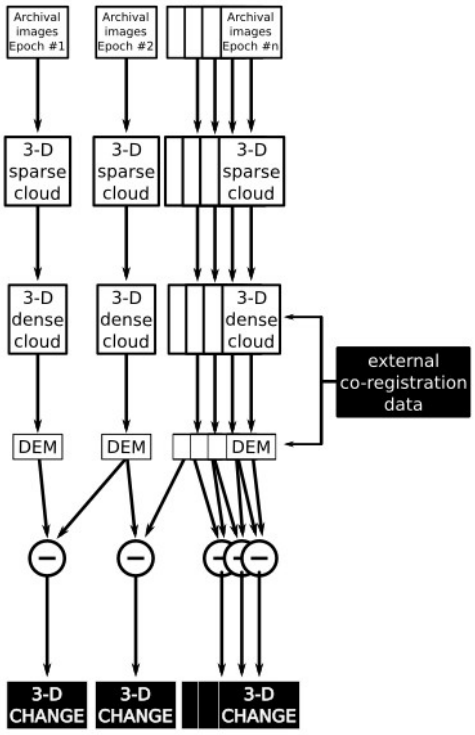

Figure 2. *Principle of 'classical' methods. Each epoch has its own geometric reference and multi-epoch Digital Elevation Models (DEM) co-registration relies on external data, such as ground control points during alignment, an external lidar DEM or even external vector data.*

1.1.3. Step-by-step description of the Time-SIFT implementation

The whole process of the Time-SIFT method can be summarized by the following three steps:

- Adjust all image orientations in a single multi-temporal block
- With image orientations fixed, split the block by epochs
- For each epoch, compute dense cloud, DEM and/or orthoimage

At the end of these three steps, the resulting 3-D data or orthoimages of the different epochs are perfectly stackable given that block geometry was estimated in a single step with all multi-temporal data and that this geometry was not changed during the following steps of dense image correlation and image mosaicking. The following sections details the Time-SIFT process.

1.1.3.1. Multi-epoch Image orientations in a single multi-temporal block

This first step is the core of the Time-SIFT method. All images of the same scene, taken at different epochs, are processed together to find homologous points and estimate cameras orientations. SfM algorithms first detect salient feature points, then match them and then eliminate outliers, using RANdom SAmple Consensus filtering (RANSAC, Fischler and Bolles 1981). With the image orientations, SfM methods estimate and iteratively refine camera positions and angles, and resulting in a sparse 3-D point cloud. The underlying prerequisite of the Time-SIFT method is there should be a majority of feature points that are stationary between two successive epochs, even if they are not found in other epochs of the study. There probably is a relationship between space and time scales for stationary features as they would probably be kept for longer time spans when the imagery is of coarser resolution and covers larger spatial domains. When using the Time-SIFT method to monitor a changing phenomenon, we recommend that the whole image dataset covers an area containing enough stable zones and avoid a strong focus on the zone of change only (see for example the “soil bulk density” case study, where images were purposely taken to be processed with the Time-SIFT method).

As the final step, the image block geometry is refined (for instance with the use of some ground control points in order to perform lens autocalibration) and - if not already done - absolute orientation is estimated. At the end of this step the final orientation of each image is obtained and will remain fixed for the whole workflow.

1.1.3.2. Split of the multi-temporal block into individual blocks (one block by epoch, image orientations kept fixed)

Proper implementation of this simple step is critical for the application of Time-SIFT method. The multi-temporal block is split into different blocks, one for each epoch, which are then processed independently. In other words, the image block geometry must not be changed after this step otherwise the datasets of different epochs would lose their intrinsic co-registration. In practice this results in a critical bottleneck in the workflow: the estimation and refinement of the cameras

orientations and lens autocalibration must be done *before* the multi-temporal block split step and not changed afterwards.

1.1.3.3. Dense cloud, Digital Elevation Model (DEM) and/or orthoimage computing for each epoch

Once the multi-temporal block is split, the workflow returns to a classical photogrammetric workflow: within each individual epoch, dense image correlation is computed. This step allows to obtain a dense 3-D point cloud. The same process is repeated for each epoch. Depending on the requirements, these dense clouds, but also interpolated DEMs and/or orthomosaics can be computed and exported. These output dataset, although coming from different epochs, share the same geometric reference and can thus be directly compared.

1.2. Case studies

To demonstrate the ability for the Time-SIFT method to produce coherent multi-temporal dataset in various situations, we present five distinct case studies. These studies differ in many ways, but are selected specifically for the following characteristics: (i) the spatio-temporal scales of the image datasets (Figure 3); (ii) relative magnitude and spatial patterns of the expected changes; (iii) different data sources; (iv) varied target phenomena.

For each case study, the following elements are given: aim of the study, dataset description, results of the Time-SIFT method associated with its added value. For the sake of simplicity, we used a single software editor (Agisoft packages Photoscan Pro® version 1.2.6 and MetaShape Pro® version 1.5.x) for applying the Time-SIFT method to each case study. We hence computed the very same processing metrics for each dataset and were hence able to compare directly these metrics. This said, it must be noted that the method can be implemented in any SfM software as demonstrated for instance through the recent application of the Time-SIFT method with MicMac by (Filhol *et al.* 2019), PhotoModeler by (Parente *et al.* 2021) or the work of (Cook and Dietze 2019).

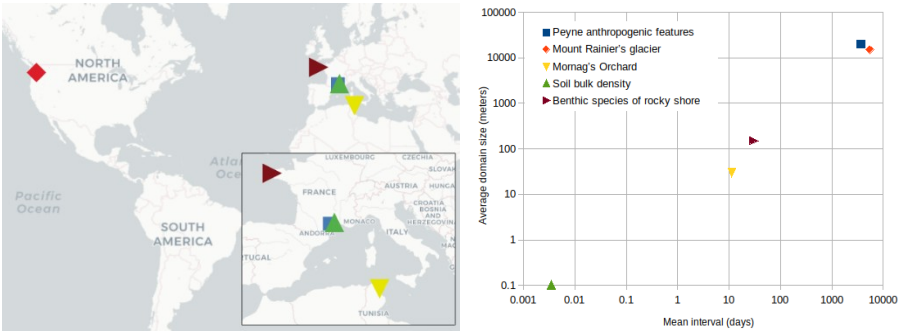

Figure 3. *Main characteristics of the case studies: A) locations and B) scales*

1.2.1. La Peyne

1.2.1.1. Objective

This case study concerns the change in land management in a Mediterranean area due to anthropogenic activity, such as urban growth, civil engineering around highways, quarries and backfills. The process of land use change followed progressive loss in land and a growth of urbanisation over the past 50 years (Vinatier and Arnaiz 2018). On a zone of several square kilometers studied by (Vinatier and Arnaiz 2018), 77% changed within fifty years. For estimating changes in urban structures over this time span, a one-meter resolution DEM is used and a call to archival aerial imagery for covering this long time period is needed. The process of attributing ground control points to sets of aerial images is very time consuming, making the use of Time-SIFT method appropriate for the documentation of past changes.

1.2.1.2. Case description

This case was the first test of the Time-SIFT method and is reported with more detail by (Feurer and Vinatier 2018a; 2018b). On a 170 km² rectangle corresponding to the lower part of the Peyne catchment (Occitanie, southern France), investigated earlier in (Vinatier and Arnaiz 2018), a part of the aerial imagery archive was downloaded (43° 35′N, 3° 19′E). The French geographic institute (IGN) provides free access to this archive through the https://remonterletemps.ign.fr/ website. Images are scanned with photogrammetric-grade scanners. The landscape is typical of Mediterranean agricultural areas dominated by vineyards and to a smaller extent,

forests. Images of the 1971, 1981, 1990, and 2001 aerial campaigns were used. Estimated Ground Sampling Distance of the images vary between 37 and 69 cm (Table 1). Nine ground control points spread over the whole area were extracted from corresponding orthorectified imagery available online (http://www.geoportail.gouv.fr) and manually picked in the images.

Epoch (date)	Images (#)	Focal length (mm)	Approximate scale	Scan resolution (µm)	Ground sampling distance (cm)
1971/06/21	61	152	1:18000	21	37
1981/06/16	27	153	1:32000	21	66
1990/06/25	31	153	1:32000	21	69
2001/06/04	44	153	1:2600	21	55

Table 1: *Parameters of scanned aerial images used in La Peyne case study*

1.2.1.3. Application of Time-SIFT method

The Peyne case study was processed with Photoscan 1.2.6 for which the handling of fiducial marks was not yet possible. Archival aerial images were first resampled with the Micmac software (Rupnik *et al.* 2017) so that fiducial marks were positioned in the corners in the resulting image. More details can be found in (Feurer and Vinatier 2018a; 2018b). As a result, pre-processed images share the same geometry and internal orientation has been taken into account before the SfM processing, which was realised with the parameters shown in Table 2.

Processing step	Property	Value
Alignment*	Accuracy	Highest
	Pair preselection	Disabled
	Key point limit	100,000
	Tie point limit	50,000
	Adaptive camera model fitting	No

Camera calibration	Camera groups	Split by epoch
Optimization	Lens parameters	f, b1, b2, cex, cy, k1, k2, k3, k4, p1, p2
	Marker accuracy (pix)	5
	Marker accuracy (m)	20
	Tie point accuracy (pix)	1
Dense cloud	Quality	High
	Depth filtering	Moderate
Mesh	Surface type	Arbitrary
	Interpolation	Enabled
	Quality	Medium
	Depth filtering	Moderate
DEM	Pixel size (m)	1
	Interpolation	Enabled

Table 2: *Time-SIFT parameters in La Peyne case study. *the sparse cloud is obtained after the "alignment" step*

1.2.1.4. Results

Application of the Time-SIFT method resulted in 4 stackable DEMs and orthophotos, represented on the right of Figure 4. Quality of image orientations can be assessed through the Root Mean Square (RMS) reprojection error values, which fall within the pixel size for all four epochs (Table 3). Quality of DEM co-registration can be investigated by comparing topographic profiles (Figure 4, bottom).

Epoch	**Dense Cloud (points)**	**Dense Cloud (pts/m^2)**	**DEM (m/pixel)**	**RMS reprojection error (pixel)**
1971	4.26 x 10^8	2.08	0.69	0.82
1981	2.20 x 10^8	0.61	1.28	0.59
1990	2.30 x 10^8	0.57	1.33	0.63
2001	2.01 x 10^8	0.87	1.07	0.68

Table 3: *Digital elevation models obtained with Time-SIFT for La Peyne*

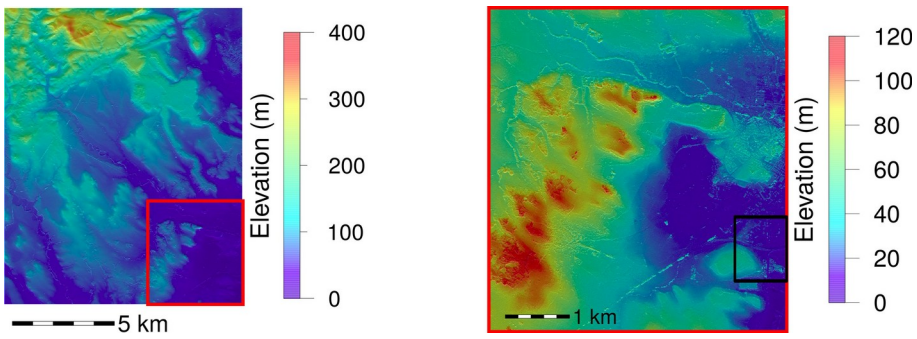

Figure 4. *Full digital elevation model of the La Peyne test site (left) and zoomed-in view (right). The black box on the right corresponds to the zone described on Figure 5 next*

Several features are apparent on the topographic profiles (Figure 4). The left part corresponds to an area where no civil engineering took place. It also seems, from orthoimage analysis, that there were no major vegetation changes. This part can then be considered as a stable zone, with possible minor changes due to limited vegetation variation. This part of the profile allows to estimate the remaining noise level : this noise is of several meters. Moreover, as already stated in (Feurer and Vinatier 2018a; 2018b), this level of noise is confirmed by the fact that new buildings are clearly visible in the successive DEMs, some of them being single-story. The right part of the profile focuses on an area that was strongly modified through time, with the construction of a highway and an interchange. Coincidentally, 1990 images were taken when the highway construction was ongoing and the north/south bridge was not present yet, which is clearly visible both on the 1990 DEM and orthoimage. The 1990 DEM seems to be a little more noisy than others. This may be related to the fact that this DEM was built from relatively coarser images (Tables 1 and 3). Conversely, the part of the 2001 DEM profile that correspond to the highway is relatively even, which indicates that the 2001 DEM is less noisy.

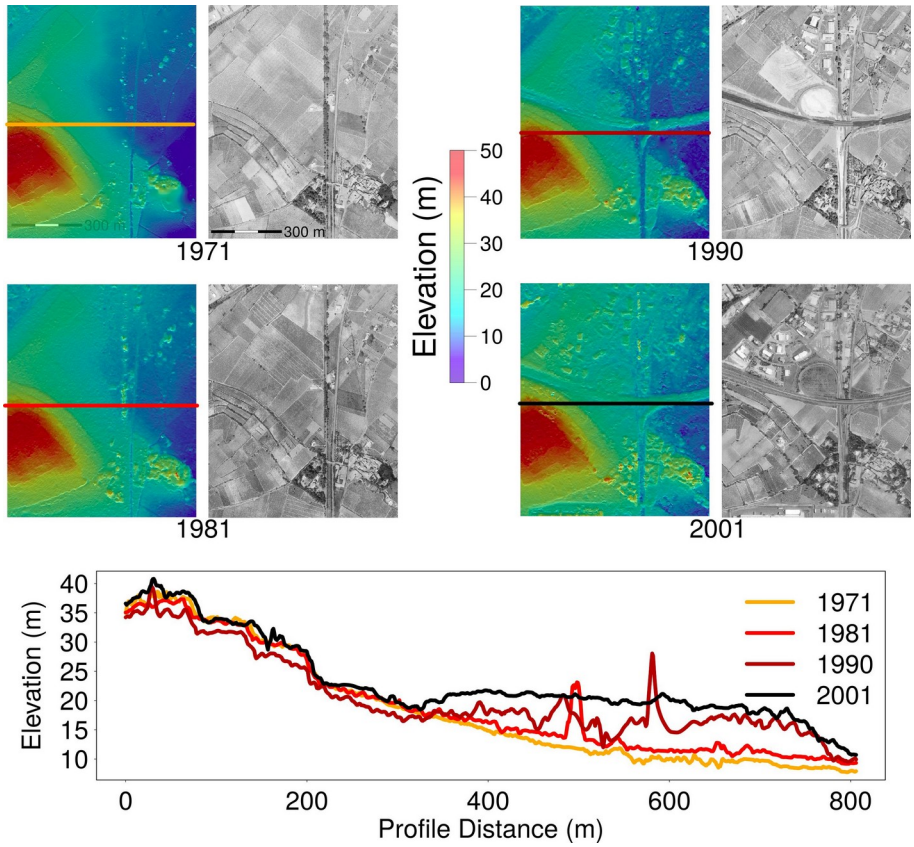

Figure 5. *La Peyne test site. Zoomed-in views of the 4 digital elevation models and orthophotos (top) with profiles extracted over the highway construction zone (bottom). The highway construction is visible on the right part of the profile.*

The most interesting finding of this test case is that, with almost only image information, one can virtually explore the whole archive of aerial imagery. In this study, only nine Ground Control Points (GCP) were used to estimate absolute orientation and scale of the 3-D models produced from 27 - 61 images by epoch, but it demonstrates that this work may be extended to wider areas and longer time spans,

provided that the required imagery is available. As shown in (Feurer and Vinatier 2018a; 2018b), the only requirements are that images were scanned with photogrammetric-grade scanners and that fiducials marks are present in the images. All the remaining processing can be done with image information only. Absolute scaling and georeferencing may even be done afterwards.

1.2.2. Mount Rainier

1.2.2.1. Objective

The processes and rates of glacier retreat and advance depend on a complex balance of environmental and climatic parameters. Even with the well-established 20th and 21st century general trend of glacial retreat, regional climatic variations and local site conditions have produced short-term glacial advances and changes in mass balance. The glaciated active volcanoes of the northwestern United States, including Mount Hood, Mount Rainier, and Mount Baker, provide a unique opportunity to examine the relationship between decadal-scale climatic patterns and local site conditions, such as aspect and elevation. Climate variability associated with the Pacific Decadal Oscillation (PDO; Mantua and Hare 2002) exerts a strong control on temperature and precipitation trends in the northwestern portion of North America (e.g., Josberger *et al.* 2007), with the 'warm' phase of the PDO leading to higher average temperatures and thinner cumulative snowpack and the 'cool' phase leading to lower average temperatures and deeper cumulative snowpack. Over the past 100 years, the PDO has exhibited a pattern of 20 to 30-year long periods of being in either the warm or cool phase (Newman *et al.* 2016). In this time period, the warm phases persisted from ~1925-1947 and again from ~1977-1998, with an intervening cool phase from ~1947-1977. Understanding changes in glacial mass balance as it corresponds with these climate variations will improve models of glacial response to future climate changes.

1.2.2.2 Case description

To improve the temporal availability of high-resolution topographic data for use in measuring the mass balance of the glaciers across major shifts in the PDO, we tested the Time-SIFT methodology on archival aerial image collections from Mount Rainier, a 4,392 m tall glaciated volcano located in the state of Washington in the United States (46.85° N, 121.75° W). Mount Rainier has 26 major glaciers occupying its flanks and 93 km^2 of permanent snowfield and glacier coverage. We

selected Mount Rainier for this case study due to the availability of snowfall records extending back to 1920, previous studies of glacial mass balance, multiple generations of publicly-available aerial images extending back to 1955, and full coverage by airborne lidar surveys in 2007-2008.

Using only aerial images that provide full coverage of Mount Rainier and are freely available (https://earthexplorer.usgs.gov/), we assembled image collections from 1955, 1970, 1983, and 1984. Adding in the 2007/08 airborne lidar, topographic data from these time spans will provide several important qualitative and quantitative tests. For one, (Sisson *et al.* 2011) used digital elevation models based on topographic maps derived from the 1970 aerial images and differenced these with the 2007/08 lidar data to measure the elevation change of glacier surfaces across the whole mountain. Measuring these elevation changes using the same datasets via the Time-SIFT method will provide a key reproducibility test. Another test follows the observed and expected trends of glacial advance and retreat, with 1955 and 1970 occurring in the middle of a cool PDO phase, and 1983 and 1984 following the transition from a cool to warm PDO phase. Accordingly, glacial volume increases from 1955 to 1970 followed by volume loss from 1970 to 1983/84 and 2007/08 would be consistent with observations. Another test of reproducibility is the 1-year interval between the 1983 and 1984 aerial image collections. If the Time-SIFT methods are producing properly scale and referenced models, the elevation differences between 1983 and 1984 should be proportionally small relative to the longer time intervals.

Epoch (date)	Images (#)	Focal length (mm)	Approximate scale	Scan resolution (µm)	Ground sampling distance (cm)
1955/09/02*	16	153.69	1:66000	25	158
1955/09/18*	10	153.69	1:66000	25	158
1970/09/09#	12	152.45	1:38000	25	150
1970/09/26#	31	152.45	1:38000	25	150
1983/08/21	18	208.401	1:58000	25	142
1984/08/25	23	208.047	1:58000	25	154

Table 4*: Parameters of scanned aerial images used in Mount Rainier case study. *Both sets of 1955 images were collected 16 days apart by the same camera and are*

processed in this study as a single epoch. # Both sets of 1970 images were collected 17 days apart by the same camera and are processed in this study as a single epoch

1.2.2.3. Application of Time-SIFT method

For Agisoft Metashape Pro, in order to recognize multiple images as being from the same camera, the digital images must have the same pixel dimensions. Our images were delivered with small variations in pixel dimensions within individual epochs. Prior to loading the images into Agisoft Metashape Pro (v. 1.5), we processed all images to trim excess pixels from the margins to ensure equal pixel dimensions for all images in each epoch. Within Metashape Pro, we defined camera groups, added calibrated focal length data from the respective calibration reports, masked the margins of the images, and then implemented the built-in fiducial mark calibration features. For several 1955 images, we had to mask out large portions of the image due to small cracks in the source film that is apparent in the scanned image. To calibrate the photos, we manually marked 4-8 fiducial marks on each image and calibrated each camera group individually. We did not perform fiducial mark-based calibrations during our initial trials of this technique, and this produced widespread topographic artifacts due to minor warping of the source film/images.

Following Time-SIFT procedures, we performed the alignment and optimization of all images in a single multi-epoch block, using the parameters listed in Table 5. With the availability of airborne lidar, we chose to use that dataset as the ground control source in our study to facilitate direct comparison of the photogrammetric DEMs with the lidar DEMs. We established 25 GCPs, using features identifiable both on the lidar topography and on the aerial imagery. These GCPs were marked manually on all images where they could be identified, and based on the size and type of features that we used as markers, we estimate that their locations were identified to within 4 m. Following the optimization step, the initial multi-epoch block was duplicated to create separate image blocks for each epoch - 1955, 1970, 1983, and 1984, respectively. Both 1955 and 1970 epochs include images collected on two different days, but because the collection was only ~2 weeks apart and taken with the same camera and approximate scale, we combined both days as a single epoch. We then produced dense point clouds, orthomosaics, and DEMs for each individual epoch and calculated DEMs of Difference (DoDs, e.g., Chandler, and Brunsden 1995) in ArcGIS (Table 6).

Processing step	Property	Value
Alignment	Accuracy	Medium
	Pair preselection	Yes
	Key point limit	100,000
	Tie point limit	50,000
	Adaptive camera model fitting	Yes
Camera calibration	Camera groups	Split by epoch
Optimization	Lens parameters	f, b1, b2, cx, cy, k1-k3, p1, p2
	Marker accuracy (pix)	5
	Marker accuracy (m)	4
	Tie point accuracy (pix)	2
Dense cloud	Quality	High
	Depth filtering	Moderate
DEM	Pixel size (m)	4
	Interpolation	Disabled

Table 5. *Time-SIFT parameters in Mount Rainier case study*

Epoch	Dense Cloud (points)	Dense Cloud (pts/m^2)	DEM (m/pixel)*	RMS reprojection error (pixel)
1955	1.26 x 10^8	0.1	4	1.08
1970	2.18 x 10^8	0.279	4	1.10
1983	1.26 x 10^8	0.124	4	1.05
1984	1.37 x 10^8	0.105	4	1.04
* DEMs were initially built at the default resolution recommended by Agisoft Photoscan Pro and later resampled to equal resolutions in ArcGIS				

Table 6. *Digital elevation models obtained with Time-SIFT for Mount Rainier*

1.2.2.4. Results

The visual derivative products from our Time-SIFT analysis on Mount Rainier, including orthomosaics, shaded-relief maps, and slope maps, provide a simple, first-order check on the quality of the topographic reconstructions. When viewed sequentially, the glaciers are the only features moving horizontally on the landscape, with the areas between glaciers remaining stationary through each time interval as expected. For more quantitative assessments of reconstruction accuracy, we examined DEMs of difference (DoDs) for different time intervals to compare our Time-SIFT derived measurements of ice thickness change to other studies of ice thickness change, known climatic patterns and geologic events, and the patterns of measured elevation change associated with geologically stable regions.

To compare our Time-SIFT results to the (Sisson *et al.* 2011) study of ice volume change spanning 1970 to 2007/08, we created a DoD from the LiDAR DEM and our 1970 DEM, clipping it to the outlines of the 2007/08 glacier extents and visualizing it with the same color scale as the previous study (Figure 6 and 7). Despite areas of missing data from the 1970 DEM in the higher elevations, general patterns of glacier advance/retreat and surface elevation changes are consistent between datasets. One notable pattern from this whole mountain perspective is that only two glaciers on the northeast slopes of Mount Rainier show cumulative advance from 1970 to 2007/08, the Winthrop and Emmons glaciers (Figure 6 and 7).

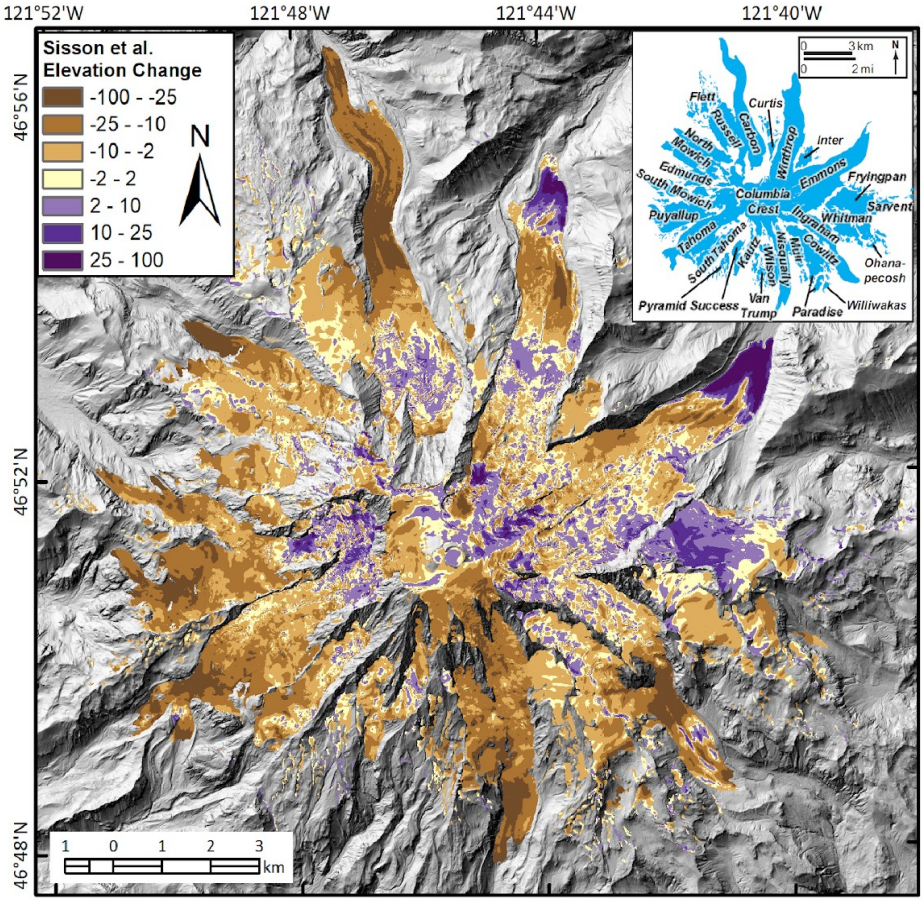

Figure 6. *Comparison of ice thickness change for all glaciers on Mount Rainier between 1970 and 2007/08 as measured by previous study of Sisson et al. (2011) which differenced digital elevation models digitized from topographic maps derived from 1970 aerial images with airborne LiDAR collected in 2007 and 2008..*

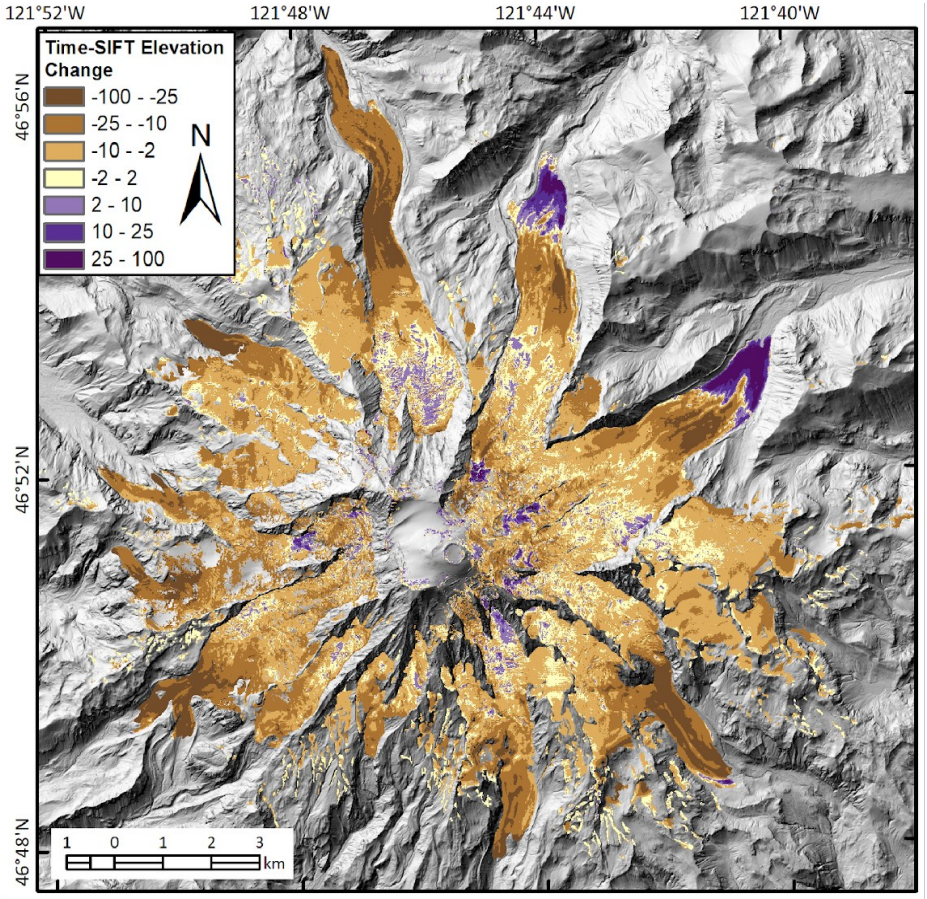

Figure 7. *Comparison of ice thickness change for all glaciers on Mount Rainier between 1970 and 2007/08 as measured by Time-SIFT-derived digital elevation model from 1970 aerial images and the same airborne LiDAR. Note the missing regions near the summit where the 1970 epoch of our Time-SIFT analysis did not resolve topography, likely due to high reflectivity and limited textural difference of the snow-covered surfaces.*

For a finer-scale view of glacier change through time, we take a closer look at the Emmons Glacier (Figures 6, 7 and 8). Examining the DoDs for our four time intervals, 1955-1970, 1970-1983, 1983-1984, and 1984-2007/08, the glacier

terminus advanced by ~1 km from 1955 to 1983, followed by relatively minor retreat of ~0.1 km from 1984-2007/08. The timing of this significant glacial advance is consistent with the 1947-1977 cool phase of the Pacific Decadal Oscillation (PDO). Although the Emmons Glacier does not show significant glacier retreat during the subsequent 1977-1998 warm PDO phase, it does exhibit significant thinning along the length of the glacier (Figure 8C and 8D) that is consistent with the expected ice loss during a PDO warm phase. Another known elevation change associated with the Emmons Glacier is the occurrence of a large rockfall event in December 1963, where an estimated 11 million cubic meters of rock collapsed from a peak on the south side of the Emmons Glacier, sending debris and mudflows across the glacier and down the valley below (Crandell and Fahnestock 1963). The effects of this event are clearly visible in the 1955-1970 DoD, where a dark red zone on southern edge (Figure 8C) shows a focused zone of elevation loss located just south of the glacier margin at a location consistent with the known rockfall origin. Further evidence of this rockfall is located downstream from the glacier (northeast corner of 1955-1970 DoD, Figure 8C) where the rockfall and mudflow deposits partially filled the main valley channel and partially eroded the young moraine deposits on the valley margins (Crandell and Fahnestock 1965). The stable terrain outside the glaciers, and in particular the regions above treeline and below late summer snowpack, provide an estimate of the ‘noise’ present in the Time-SIFT DEMs of this case study. For example, a sparsely vegetated valley to the north of the Emmons Glacier exhibits topographic noise on the order of ~2 meters. Steeper terrain and vegetated regions exhibited higher variability, likely due to differences in how trees are resolved or filtered in different epochs and variations in illumination in high-relief zones.

This case study demonstrates that the Time-SIFT methodology provides a valuable, robust, and efficient strategy for the production of co-registered DEMs from the wealth of archival aerial imagery over this large area (>400 km^2). While numerous studies of glacier mass balance have documented the more easily measured quantity of glacier extent from archival aerial images as a proxy for glacier mass balance, our results show that a glacier can experience significant mass loss through thinning without a remarkable change in terminus position. This observation emphasizes the potential of Time-SIFT in assisting, with the extraction of richer 3D historical datasets, for quantifying historical geologic and geomorphic change.

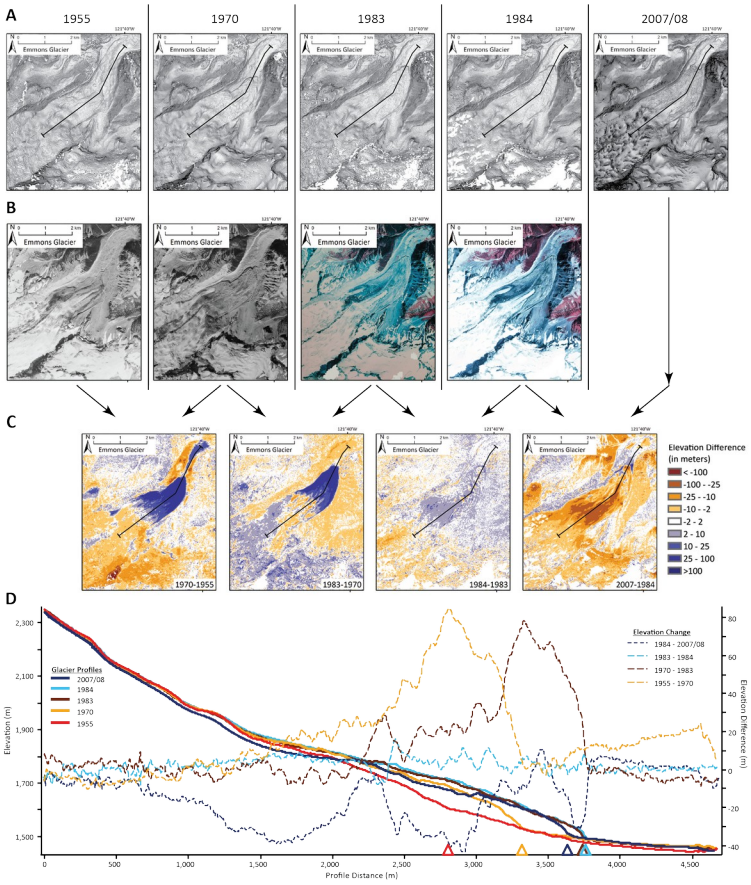

Figure 8. *Analysis of Time-SIFT derived digital elevation models of the Emmons Glacier on Mount Rainier. (A) Slope-maps of the lower Emmons Glacier for each Time-SIFT epoch and the 2007/08 LIDAR data. (B) Orthoimages of the lower Emmons Glacier for each epoch. (C) elevation changes that occurred in the time intervals between each Time-SIFT epoch and the LIDAR data. (D) Topographic profiles of the Emmons Glacier surface for each epoch (left axis) and the corresponding elevation difference between epochs (right axis). Triangles along the x-axis denote the glacier terminus positions and are color-coded for the respective epoch. The elevation changes illustrate significant glacial advance and thickening below 1900 m elevation from 1955 to 1983. From 1984 to 2007/08, the terminus experienced only minor retreat, but saw significant thinning along much of its length, especially below 2000 m.*

1.2.3. Mornag's orchard

1.2.3.1. Objective

In the technical management of orchards, farmers need to optimise both the quantities of water used for irrigation and the quantity of crop protection products. These quantities directly influence tree development. One of the widespread indicators used to monitor plant and tree development is the Leaf Area Index, a dimensionless quantity computed as the ratio between leaf area and the related ground area. Water demand is indeed directly related to the amount of foliage, with evapotranspiration occurring through the leaf stomata. Similarly, the need for crop protection product is directly related to the surface area of the foliage.

However, methods for estimation of Leaf Area Index only exist at the punctual scale, either through dedicated measuring devices, by processing images obtained with hemispherical cameras, or at the field scale, with earth observation image processing. (Mabrouk *et al.* 2017) report a study where a UAV was used to acquire very high resolution 3-D data on a peach orchard in Mornag, Tunisia, in order to test the ability of such data to provide Leaf Area Index time series. This test case is based on the data gathered for that study. In the original study, no absolute geometric reference was given to the 3-D dataset and only a relative orientation was obtained. The 3-D models were given a correct scale by using targets of known dimensions, installed in the investigated scene. Each epoch was processed separately and the 3-D point clouds were not stackable. The use of the Time-SIFT method may therefore make it possible to monitor the tree and canopy growth at the scale of the individual tree.

1.2.3.2 Case description

The farm is located in Khelidia, near Mornag, Ben Arous governorate, Tunisia (36°39'50"N 10°12'32"E). This region has a semi-arid climate with mild winters and hot summers. The field plot on which the experiment was conducted is a 0.77 ha field planted in 2010 with peach trees of the Sweet Cap variety.

In total, 5 image acquisitions at 5 different epochs of the first semester of the year 2015 were done. Flights plans were conducted at low altitude (between 10 and 30 meters) with nadir and oblique images in order to favor the rendering of the tree crowns (see Table 7). The ancillary data used in (Mabrouk *et al.* 2017), which

consisted in targets of known dimensions installed at different places for each acquisition, were not used for this case study.

Epoch (date)	Images (#)	Flying height (m)	Focal length (mm)	Approximate scale	Ground Sampling Distance (cm)
2015/04/20	107	24.8	8.8	1:2818	0.61
2015/05/05	581	11.6	8.8	1:1318	0.32
2015/05/15	96	15.3	8.8	1:1738	0.31
2015/05/26	205	12.7	8.8	1:1443	0.33
2015/06/04	209	14.7	8.8	1:1670	0.33

Table 7. *Image dataset parameters for the "Mornag's orchard" study*

1.2.3.3. Application of Time-SIFT method

For this test case, all images were acquired with the same UAV and the same camera. As a result, all images were imported in a single multi-temporal block. Unfortunately, considering both the grass growth between the trees and the tree growth (mainly, leaf growth and increased leaf coverage), the first attempts resulted in missed orientations for some of the images or epochs within the multi-temporal block, depending on the tested parameters. Therefore, a trial-and-error approach was adopted until a functional set of values for the Photoscan parameters was found. It appears that increasing the number of desired tie points allowed for the success of the orientation of all images of the multi-temporal block, which is depicted in Table 8.

Processing step	Property	Value
Alignment	Accuracy	High
	Pair preselection	No
	Key point limit	40,000
	Tie point limit	40,000
	Adaptive camera model fitting	Yes

Camera calibration	Camera groups	Split by epoch
Dense cloud	Quality	High
	Depth filtering	Moderate
DEM	Pixel size (m)	0.01
	Interpolation	Enabled

Table 8. *Time-SIFT parameters in Mornag's orchard case study*

1.2.3.4. Results

Once the alignment of the whole block was achieved, alignment quality was found to be quite good, with reprojection error of approximately 0.5 pixel (Table 9). These results were favored by the fact that oblique imagery was acquired at each epoch, ensuring a better estimation of image block geometry (James *et al.* 2019). It is also worth noting that if point cloud density is lower (and DEM resolution coarser) for the first acquisition, done at a higher altitude, the RMS reprojection error stays within the same range as other epochs, which relates well with the multi-scale robustness of the Time-SIFT method.

Epoch	**Dense Cloud (points)**	**Dense Cloud (pts/m^2)**	**DEM (m/pixel)**	**RMS reprojection error (pixel)**
2015/04/20	32.0 x 10^6	6 650	0.0120	0.53
2015/05/05	95.6 x 10^6	23 700	0.0065	0.50
2015/05/15	39.4 x 10^6	26 400	0.0065	0.43
2015/05/26	77.9 x 10^6	22 300	0.0067	0.47
2015/06/04	63.4 x 10^6	22 700	0.0064	0.51

Table 9. *Time-SIFT results for Mornag's orchard*

In terms of thematic results, having perfectly stackable point clouds, DEMs and orthophotos allow for a detailed 3-D monitoring at the tree scale. Indeed, when examining the DEMs at the tree level, one can clearly see the canopy development through the growing season, with branches growing and being covered by more leaves through time (Figure 9). It is worth noting that no ground information was

used to obtain these results. Scale of the 3-D models was provided by the GPS position recorded onboard the UAV and apart from this information, only image information was used in the processing. This example proves that the Time-SIFT method can be used to apply a very light protocol that allows to monitor tree crops at the tree scale. In the previous studies based on the same dataset, (Mabrouk *et al.* 2018) showed that this kind of information may be favorably used to pilot the irrigation and/or pesticide application scheme.

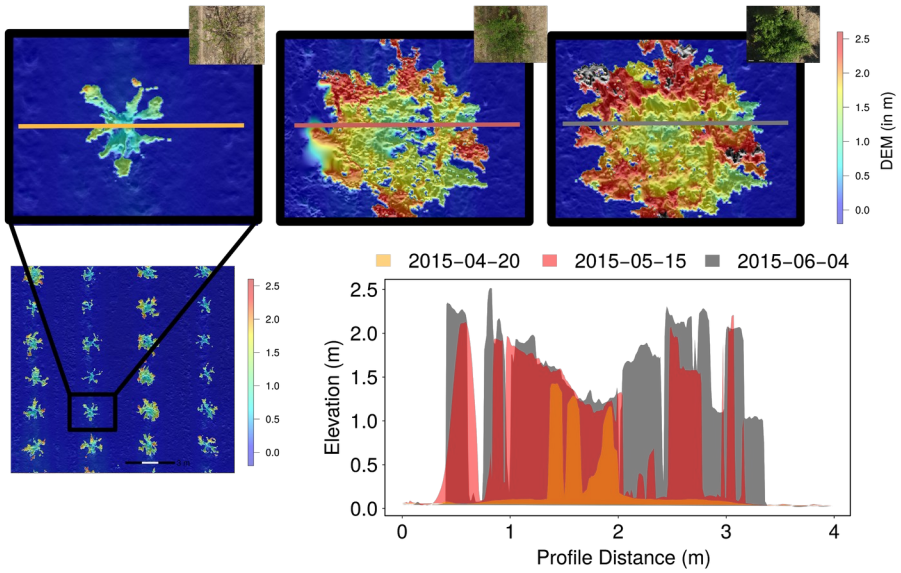

Figure 9. *Monitoring of a single tree crown development. Plan views of a digital elevation model (bottom left) with zoomed views at 3 dates (top) and extracted profiles (bottom right). Tree development within this time period mainly consists of foliage growth.*

1.2.4. Soil bulk density

1.2.4.1. Objective

In soil studies, especially for the monitoring of hydrological processes, soil bulk density is one of the major physical parameters. Among the existing methods, the core sampling method relies on the use of a metal cylinder with a known volume

(most often 100 cm^3) that is hammered into the target soil horizon. The soil sample is then dried and weighed in lab, with the bulk density calculate by dividing this mass by the sample volume. This is the most common method due to its efficiency; however, core sampling cannot be applied in all sediments, such as when the soil is too pebbly. In these cases, pedologists rely on the use of other methods which are based on the estimation of soil sample volumes. These methods share the same requirement: volume estimation must be done from the top of the soil horizon, which in turn requires the investigator to excavate the soil until the desired horizon. We investigate a new method for estimating sample volumes for bulk density measurements using photogrammetry. In simple terms, the protocol is to create a 3-D model of the investigated soil horizon *before* and *after* a sample is excavated, with the volume of the soil sample being the difference between both models. In order to minimize the need for external data, we implement the Time-SIFT method to obtain a direct co-registration of both 3-D models. Hence the required field material is limited to a camera and targets of known dimensions used to scale the 3-D models.

1.2.4.2. Case description

We dug a soil pit on 2018/10/01 in the experimental fields of the French National Research Institute for Agriculture, Food and Environment (INRAE, formerly INRA) near Mauguio (43°36’30” N 3°58’56” E) and described the soil profile following the guidelines for soil description (FAO 2006). The soil corresponds to a fluvisol (WRB 2015) and is mainly characterized by a sandy clay loam texture, medium subangular blocky structure, and a high discernible porosity.

Our field protocol followed these steps: 1) fix four scales of known dimensions around the investigated zone, 2) acquire convergent images spanning the target area, 3) excavate five separate samples from different locations on the target surface, 4) acquire a second set of convergent images was done (see Table 10 for the acquisition parameters). The four targets of known dimension provide the scale to the 3-D model and were not moved between image acquisitions. To validate our results, we also collected 3 core samples to allow us to compare this method with the traditional approach.

Epoch (time) 2018/10/01	Images (#)	Acquisition distance (m)	Focal length (mm)	Approximate scale	Ground Sampling Distance (cm)
13:27	34	1	18	1:55	0.02
13:55	43	1	18	1:55	0.02

Table 10. *Image dataset parameters for the "soil bulk density case" study*

1.2.4.3. Application of Time-SIFT method

For this case, the Time-SIFT multi-temporal block contains only two epochs separated by 28 minutes. Agisoft Photoscan Pro automatically detected the targets and we input scale information using these targets after image alignment. We split the aligned block into separate before and after blocks for subsequent dense construction. The convergent acquisition favored accurate lens autocalibration. We retained the default processing parameters; these are reported in Table 11.

Processing step	Property	Value
Alignment	Accuracy	High
	Pair preselection	No
	Key point limit	40,000
	Tie point limit	4,000
	Adaptive camera model fitting	Yes
Camera calibration	Camera groups	Split by epoch
Optimization	Lens parameters	f, cx, cy, k1-k3, p1, p2
	Marker accuracy (pix)	n/a
	Marker accuracy (m)	n/a
	Tie point accuracy (pix)	1
Dense cloud	Quality	High
	Depth filtering	Mid
DEM	Pixel size (m)	0.01
	Interpolation	Enabled

Table 11. *Time-SIFT parameters in Soil bulk density case study*

1.2.4.4. Results

The Time-SIFT method produced high-resolution, accurate models for volume calculation without any need for cumbersome parameter tuning or additional processes to co-register 3-D models. We found that systematic image collection across the full target zone, with a convergent imaging geometry is critical to capture the full details of the surface and to support the accurate estimation of lens parameters, all of which is required for high-quality SfM results. The success in lens auto-calibration is demonstrated by a reprojection error of 0.86 pixel (Table 12) and a RMSE of 0.2mm, which is the same scale as the ground sampling distance.

Epoch time (2018/10/01)	Dense Cloud (points)	Dense Cloud (pts/cm^2)	DEM (cm/pixel)	RMS reprojection error (pixel)	RMS reprojection error on scales (cm)
13:27	10.1 x 10^6	1065	0.214	0.86	0.021
13:55					

Table 12. *Time-SIFT results for Soil bulk density*

The profile view illustrates the accurate registration of the stable surfaces and the negligible noise at this scale (Figure 10). We assessed the quality of volume estimation with the Time-SIFT method by comparing with classical soil volume estimation methods. Volumes measurements between 100 and 1400 cm^3 made with the Time-SIFT method produced an RMSE of 15 cm^3 (full study details in Coulouma *et al.* 2021). The Time-SIFT methods produced mean soil bulk density of 1.53 with a standard deviation of 0.04 (n=5). These measurements are consistent with the mean bulk density of 1.59 with a standard deviation of 0.03 (n=15) obtained from the core sampling methods (Coulouma *et al.* 2021).

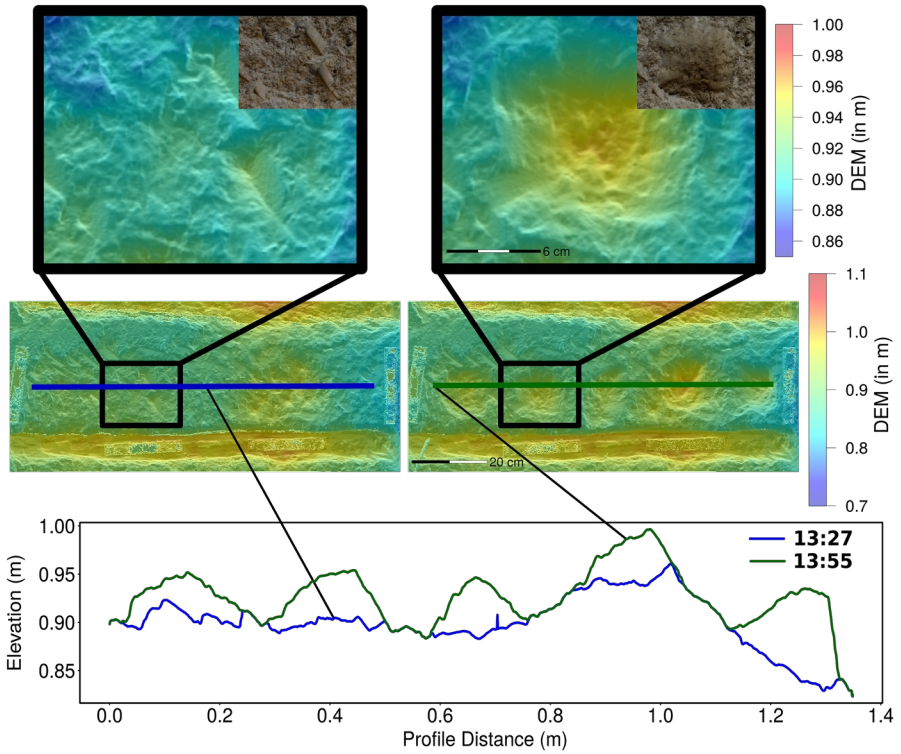

Figure 10. *Profiles of the five excavations and close-up on a single sampling site. Excavations were done in the vertical wall of the soil pit. At this scale, no difference between the two profiles can be detected on the stable zones.*

In the estimation of soil bulk density by photogrammetry, the Time-SIFT method allows the operator to follow a simplified protocol. Indeed, once the scaling targets set, the operator freely acquires a convergent set of images *before* and *after* the soil sampling without any constraint but the full stereoscopic coverage of the investigated horizon. The Time-SIFT method allows for a co-registration of the two data sets which can then be compared to estimate sample volumes only with image information and the use of scale bars.

1.2.5. Benthic species in rocky-shore

1.2.5.1. Objective

In the last decade, with the improvement of photographic and video surveys, the evaluation of species habitats at fine resolution scale (i.e., cm) has become a reality (e.g., Laliberte and Rango 2011; Ventura *et al.* 2018). This facilitates better comprehension about species habitat selection and behavior at the individual level. In complex habitats, such as the rocky shore intertidal zone in coastal ecosystems, the microtopographic features of the substrate potentially determine the population dynamics and small-scale distribution of benthic species by interacting with seasonal environmental changes (e.g. temperature, waves action, sand coverage) (Harley 2008; Gomes *et al.* 2018) and by determining inter-specific interactions (Fletcher and Underwood 1987). Intertidal rocky shore ecosystems are extremely dynamic. They are subject to many environmental factors across temporal scales from hours (e.g., tide) to years (e.g., climate-related events). To better understand spatiotemporal species distribution on complex habitats, it is thus imperative to represent the microhabitat structure by evaluating not only its static features such as the substrate roughness (Meager *et al.* 2011), but also its dynamics. Here, we aim to test the Time-SIFT methodology to evaluate its adequacy to study the population dynamics of the mussel *Mytilus sp.* in a rocky-shore intertidal area in Brittany based on a monthly survey using high-resolution aerial images taken by drone. We develop a time series of co-registered 3D models to address the following question: how does the structure and dynamics of small-scale habitat influence the distribution patterns and structure (e.g. individual size, density) of mussel population?

1.2.5.2. Case description

The monitored rocky-shore area is located in *Le Petit Minou* beach, close to the semi-enclosed coastal Bay of Brest (Western Brittany, France) (48°20’19”N 4°37’03”W). This location presents diverse features and is influenced by the dynamics of the beach environment, which changes through time as a result of waves and tidal cycles. We used a DJI® Phantom 4 pro platform to take images at low altitude every 1 second approximately (about 15-30 m height, ground resolution: ~0.7cm, covered surface: ~7500m^2) to obtain an overlap of about 80% between consecutive images. All images were collected at low tide to reduce the effect of water in the contrast and visualization of the rocky-shore. We selected four months of drone-survey images for testing with the Time-SIFT methodology. We

seek a perfect overlap of the geographic coordinates to identify potential topographic dynamics and consequences on mussels'

Epoch (date)	Images (#)	Flying height (m)	Focal length (mm)	Approximate scale	Ground Sampling Distance (cm)
2019/02/26	90	29.3	8.8	1:3330	0.7
2019/03/22	103	28.3	8.8	1:3215	0.7
2019/05/06	156	24.5	8.8	1:2785	0.6
2019/06/05	287	15.6	8.8	1:1775	0.4

distribution. Flight parameters are reported in Table 13.

Table 13. *Flight parameters for the Rocky-shore case study*

1.2.5.3. Application of Time-SIFT method

As for the soil bulk density test case (Section 1.2.4.), application of the Time-SIFT method was straightforward, successfully producing co-registered 3D models utilizing the default parameters in Agisoft Photoscan Pro (Table 14 below). This was initially unexpected due to the seemingly high degree of change in portions of the study area, including new sand deposits and areas inundated by the sea.

Processing step	Property	Value
Alignment	Accuracy	High
	Pair preselection	No
	Key point limit	40,000
	Tie point limit	4,000
	Adaptive camera model fitting	Yes
Camera calibration	Camera groups	Split by epoch
Dense cloud	Quality	High
	Depth filtering	Moderate
DEM	Pixel size (m)	0.01
	Interpolation	Enabled

Table 14. *Time-SIFT parameters in the Rocky-shore case study*

1.2.5.4. Results

Accurate co-registration of individual epochs is illustrated by the topographic profiles in Figure 11. This is possible because all epoch images were acquired using the same planning and purpose and thanks to that each image covers both stable (rock) and changing areas (sand, mussels and sea-water). Success in lens auto-calibration is supported by the corresponding small reprojection error (Table 15).

Epoch	Dense Cloud (points)	Dense Cloud (pts/m^2)	DEM (m/pixel)	RMS reprojection error (pixel)
2019/02/26	32.0 x 10^6	6 650	0.012	0.53
2019/03/22	95.6 x 10^6	23 700	0.0065	0.50
2019/05/06	39.4 x 10^6	26 400	0.0065	0.43
2019/06/05	77.9 x 10^6	22 300	0.0067	0.47

Table 15. *Time-SIFT results for Rocky shore*

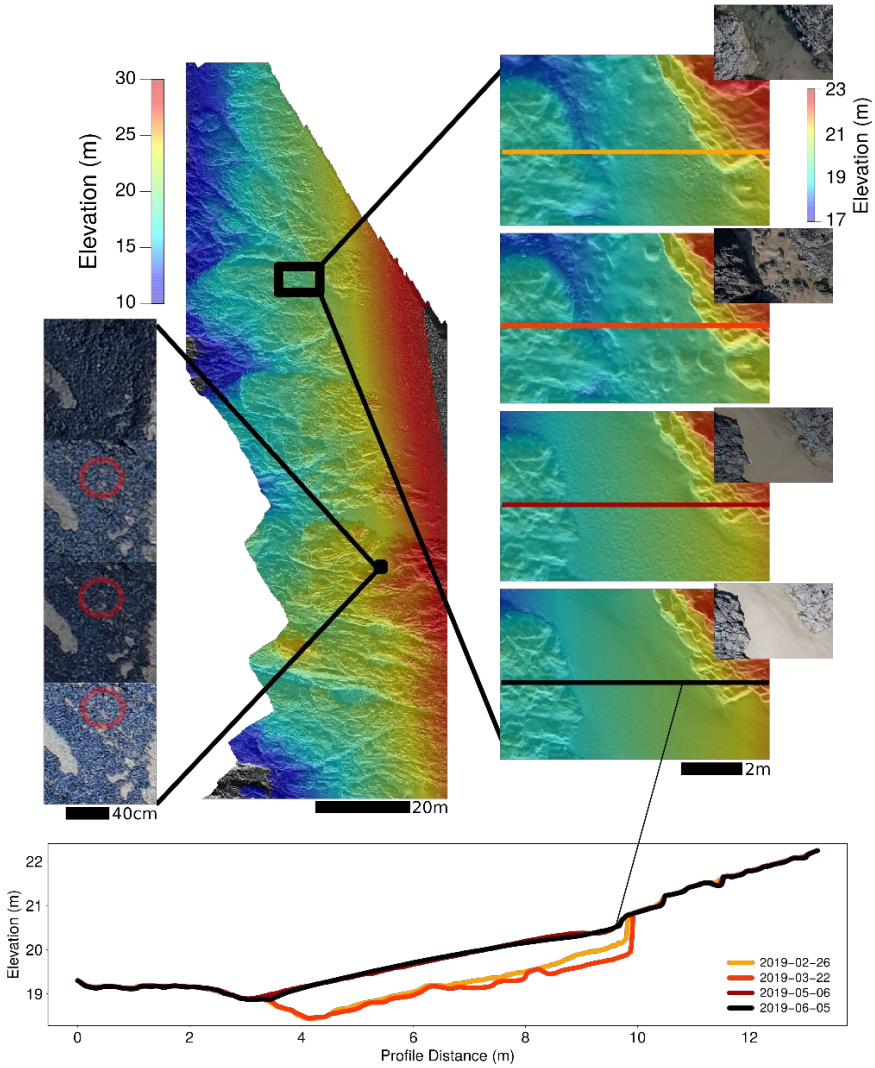

Figure 11. *Multi-temporal digital elevation models and orthophotos showing evolution of the mussel beds distribution (left) and geomorphologic changes (right and bottom). Red circles on the orthoimages indicated the disappearance of mussels in the selected area.*

The results show excellent performance of the Time-SIFT method to compare temporal variations, from centimeter to meter scales (Figure 11). Significant variations occurred in the accumulation of sand between the rocks, with accumulation during spring time, reducing the surface area of rocky habitats (Figure 11, right and bottom). Because the sand burial or a heavy load of suspended sand can stress mussels and cause mortality (Zardi *et al*. 2006), such sand inundation may have significant consequences on the studied mussel population. The geographic overlap may permit a comparison of mussel's distribution at scale of centimeters to evaluate the dynamic of mussel patches coverage and to identify and quantify the consequences of such sand mobilization on the mussel beds (orthoimages at left on Figure 11). The Time-SIFT method allows the study area to be sub-sampled and thus will provide the opportunity to compare contrasting habitats to assess whether there is a direct relationship between the evolution of topography related to sand mobilization and mussel beds distribution and evolution.

Although drone images bring an easy and cheap way to study local scale habitat features (cm) at median spatial scale (>100 m length), typically the number and distribution of ground control points determine the accuracy of the topography reconstruction of coastal linear landforms using Structure from Motion photogrammetry (Jaud *et al.* 2018). However, in coastal areas, recording the ground control points is time consuming and frequently restricted by tides and coastal topography. As a result, this setting is an important case study for the Time-SIFT method. Under these conditions and as observed in this case of study, the Time-SIFT approach facilitates high quality temporal comparison of the orthophotos and 3-D reconstructions where ground control opportunities are limited. This opens new perspectives in using archival aerial imagery and/or collecting new drone imagery for monitoring change. Quantifying the dynamics of habitat features at high-resolution is essential to better integrate small-scale processes into species distribution modelling approaches, particularly in the context of climate change and its effects on coastal ecosystems.

1.2.6. Test cases synthesis

With a successful application of the Time-SIFT method on five contrasting test cases, we derive several conclusions about the potential of this method: First,

Time-SIFT is able to handle a wide range of different spatio-temporal scales

For our five varied spatio-temporal cases, Time-SIFT succeeded in obtaining complete multi-temporal blocks. Considering that the Time-SIFT method is based almost on image information only and that it takes advantage of the invariance properties of the SIFT-like algorithms, this finding was expected. Moreover, the spatio-temporal sampling was adapted to the spatio-temporal variability of the investigated phenomena, which strongly favored the success of the Time-SIFT method. In the first case, the high level of noise, still lower than the intensity of the studied phenomena, should be reconciled to the quality of the archival images. However, for the last four cases and despite the good quality of the images, conditions of success were far from optimal considering the relative amount of change in the image time series, whether the change affected large parts of glaciers, of a cultivated orchard, of a soil pit wall with excavations or even a tidal shore with significant sand deposits. Perhaps surprisingly, adjusting the processing parameters through trial-and-error was only necessary for the Mornag's orchard test site. The reason may be that, for this test case, the change concerned not only the growing trees but also the ground coverage between the trees, where grass grew during the period of analysis. Perhaps the most remarkable result is the one obtained for the rocky shore test case. Images taken near the sea constitute a 'worst case' in photogrammetry, due to changes within epochs due to waves and that no ground control points can be set on the ocean side of the images. Second,

Time-SIFT can mitigate limitations imposed by the lack of ground control points

The test cases for Mornag's orchard (section 1.2.3.), soil bulk density (section 1.2.4.), and the rocky shore (section 1.2.5.) employed a processing routine where no ground control points were used. These studies defined the scaling for their 3-D model through the use of either the UAV GPS data or the use of an object of known dimensions in the images (soil bulk density test case). This may be one of the most powerful features of the Time-SIFT method, considering that ground control points may be difficult to obtain due to diverse factors such as the use of archival imagery, for which ground information was lost or never collected, or due to a limited accessibility to the ground. Finally, as in the "rocky shore" test case, ground control points may not be available on some parts of the covered domain simply because there is no stable ground within the target area (foreshore and areas permanently covered by the sea).

The Time-SIFT method therefore provides an unprecedented potential for unlocking the processing of stereoscopic imagery, given that absolute reference

and/or scale can be given to the multi-temporal block only after obtaining the relative orientation of the whole image dataset Third,

Time-SIFT produces robust co-registration of multiple image epochs

For all the test cases, reprojection error falls within the pixel size, or is at worst, the order of magnitude of the pixel. It means that intrinsic co-registration of the image block can be done with a precision that is given by the pixel size. This result is consistent with the known quality of the SIFT feature positioning - approximately 0.3 pixel, depending on the feature detection and matching algorithm (Appolonio *et al.* 2014). In some cases this quality may not be sufficient, such as when the target phenomena have a magnitude which is only slightly bigger than the pixel size. In these cases, the approach of (Truong *et al.* 2018) using image correlation to refine the positions of the SIFT points may provide favorably results.

Examining 2D profiles across where change has not occurred provides an extrinsic assessment of the quality of the results and an estimate of the order of magnitude of the noise in the modeled digital elevation models (DEM). For the Peyne test cases, this finding is supported by the fine DEM and coarse DEM error values quantified in (Feurer and Vinatier 2018a; 2018b).

1.3. Conclusion

In this study we proposed five test cases to demonstrate the ability of the Time-SIFT method to provide coherent multi-temporal 3-D and/or 2D datasets with limited or even without external registration data. Our results show that the Time-SIFT method consistently succeeds in the simultaneous orientation of all images of different epochs within a significant range of spatiotemporal scales. This work demonstrates that the Time-SIFT method can be successfully applied for a wide variety of cases and illustrates the range of opportunities for application of time series analysis of photogrammetrically-derived digital elevation models. Additional work could further characterize optimal conditions and primary sources of error for application of the Time-SIFT method. In particular, sensitivity analyses are required to better determine *a priori* the required set of parameters that would enable the success of the method and to determine the impact of the dataset characteristics such as the number of images by epoch, the number of epochs, or the image characteristics of each epoch.

We expect that the Time-SIFT method will help to unlock the existing multi-temporal stereoscopic image archive for abroad range of change detection studies. Candidate studies for testing the Time-SIFT method include: tracking large landslide displacements (Dewitte *et al.* 1998; Lucieer *et al.* 2014), seasonal evolution of narrow landscape elements such as ditches, hedgerows, channels (Vinatier *et al.* 2018), and documentation of structured objects such as houses or buildings. Finally, to support access to the Time-SIFT method, we plan to add it as a module to the Agisoft Metashape® software.

1.4. References

Apollonio, F. I., Ballabeni, A., Gaiani, M., Remondino, F. (2014). Evaluation of feature-based methods for automated network orientation. *International Archives of the Photogrammetry, Remote Sensing & Spatial Information Sciences* (45).

Bakker, M., Lane, S. N. (2017). Archival photogrammetric analysis of river-floodplain systems using Structure from Motion (SfM) methods. *Earth Surface Processes and Landforms* (42:8), pp. 1274–1286.

Bemis, S. P., Micklethwaite, S., Turner, D., James, M. R., Akciz, S., T. Thiele, S., Bangash, H. A. (2014). Ground-based and UAV-Based photogrammetry: A multi-scale, high-resolution mapping tool for structural geology and paleoseismology. *Journal of Structural Geology* (69, Part A), 163–178.

Brodu, N., Lague, D. (2012). 3D terrestrial lidar data classification of complex natural scenes using a multi-scale dimensionality criterion: Applications in geomorphology. *ISPRS Journal of Photogrammetry and Remote Sensing*, 68, 121–134.

Carrivick, J. L., Smith, M. W., Quincey, D. J. (2016). *Structure from Motion in the Geosciences*, John Wiley & Sons.

Chandler, J. H., Brunsden, D. (1995). Steady state behaviour of the Black Ven mudslide: the application of archival analytical photogrammetry to studies of landform change. *Earth Surface Processes and Landforms*, *20*(3), 255–275.

Chanut, M.-A., Kasperski, J., Dubois, L., Dauphin, S., Duranthon, J.-P. (2017). Quantification des déplacements 3D par la méthode PLaS - application au glissement du Chambon (Isère). *Revue Française de Géotechnique*, 150, 4.

Cook, K. L., Dietze, M. (2019). A simple workflow for robust low-cost UAV-derived change detection without ground control points. *Earth Surface Dynamics*, 7(4), 1009–1017.

Coulouma, G., Feurer, D., Vinatier, F., Huttel, O. (2021) Assessing new sensor-based volume measurement methods for high-throughput bulk density estimation in the field under various soil conditions. *European Journal of Soil Science*, 72, 2049–2061.

Cowley, D. C., Stichelbaut, B. B. (2012). Historic Aerial Photographic Archives for European Archaeology. *European Journal of Archaeology* (15:2), 217–236.

Crandell, D. R., Fahnestock, R. K. (1965). Rockfalls and Avalanches from Little Tahoma Peak on Mount Rainier, Washington. (1221-A), Technical report, U.S. Government Printing Office.

Dewitte, O., Jasselette, J.-C., Cornet, Y., Van Den Eeckhaut, M., Collignon, A., Poesen, J., Demoulin, A. (2008). Tracking landslide displacements by multi-temporal DTMs: a combined aerial stereophotogrammetric and LIDAR approach in western Belgium. *Engineering Geology* (99:1-2), 11–22.

Eltner, A., Kaiser, A., Castillo, C., Rock, G., Neugirg, F., Abellan, A. (2016). Image-based surface reconstruction in geomorphometry - merits, limits and developments. *Earth Surface Dynamics* (4:2), 359–389.

FAO (2006) *Guidelines for soil description*, Fourth edition. FAO, Rome.

Feurer, D., Vinatier, F. (2018a). The Time-SIFT method: detecting 3-D changes from archival photogrammetric analysis with almost exclusively image information. *arXiv preprint arXiv:1807.09700*.

Feurer, D., Vinatier, F. (2018b). Joining multi-epoch archival aerial images in a single SfM block allows 3-D change detection with almost exclusively image information," *ISPRS journal of photogrammetry and remote sensing* (146), 495–506.

Filhol, S., Perret, A., Girod, L., Sutter, G., Schuler, T. V., Burkhart, J. F. (2019). Time-Lapse Photogrammetry of Distributed Snow Depth During Snowmelt. *Water Resources Research* (55).

Fischer, L., Eisenbeiss, H., Kaab, A., Huggel, C., Haeberli, W. (2011). Monitoring topographic changes in a periglacial high-mountain face using high-resolution DTMs, Monte Rosa East Face, Italian Alps. *Permafrost and Periglacial Processes* (22:2), 140–152.

Fischler, M. A., Bolles, R. C. (1981). Random sample consensus: a paradigm for model fitting with applications to image analysis and automated cartography. *Communications of the ACM* (24:6), 381–395.

Fletcher, W. J., Underwood, A. J. (1987). Interspecific competition among subtidal limpets: effect of substratum heterogeneity. *Ecology* (68:2), 387–400.

Fonstad, M. A., Dietrich, J. T., Courville, B. C., Jensen, J. L., Carbonneau, P. E. (2013). Topographic structure from motion: a new development in photogrammetric measurement. *Earth Surface Processes and Landforms* (38:4), 421–430.

Giordano, S., Le Bris, A., Mallet, C. (2018). Toward automatic georeferencing of archival aerial photogrammetric surveys. *ISPRS Annals of Photogrammetry, Remote Sensing and Spatial Information Sciences* (IV-2), 105–112.

Gomes, I., Peteiro, L., Bueno-Pardo, J., Albuquerque, R., Perez-Jorge, S., Oliveira, E. R., Alves, F. L., Queiroga, H. (2018). What's a picture really worth? On the use of drone aerial imagery to estimate intertidal rocky shore mussel demographic parameters. *Estuarine, Coastal and Shelf Science* (213), 185–198.

Haas, F., Hilger, L., Neugirg, F., Umstadter, K., Breitung, C., Fischer, P., Hilger, P., Heckmann, T., Dusik, J., Kaiser, A., Schmidt, J., Della Seta, M., Rosenkranz, R., Becht, M. (2016). "Quantification and analysis of geomorphic processes on a recultivated iron ore mine on the Italian island of Elba using long-term ground-based lidar and photogrammetric SfM data by a UAV. *Natural Hazards and Earth System Sciences* (16:5), 1269–1288.

Harley, C. D. G. (2008). Tidal dynamics, topographic orientation, and temperature-mediated mass mortalities on rocky shores. *Marine Ecology Progress Series* (371), 37–46.

WRB (2015). *World reference base for soil resources 2014, update 2015*, World Soil Resources Reports No. 106. FAO, Rome.

James, M. R., Chandler, J. H., Eltner, A., Fraser, C., Miller, P. E., Mills, J. P., Noble, T., Robson, S., Lane, S. N. (2019). Guidelines on the use of structure-from-motion photogrammetry in geomorphic research. *Earth Surface Processes and Landforms* (44).

Jaud, M., Passot, S., Allemand, P., Le Dantec, N., Grandjean, P., Delacourt, C. (2019). Suggestions to Limit Geometric Distortions in the Reconstruction of Linear Coastal Landforms by SfM Photogrammetry with PhotoScan and MicMac for UAV Surveys with Restricted GCPs Pattern. *Drones* (3:1).

Josberger, E. G., Bidlake, W. R., March, R. S., Kennedy, B. W. (2007). Glacier mass-balance fluctuations in the Pacific Northwest and Alaska, USA. *Annals of Glaciology* (46), 291–296.

Laliberte, A. S., Rango, A. (2011). Image processing and classification procedures for analysis of sub-decimeter imagery acquired with an unmanned aircraft over arid rangelands. *GIScience & Remote Sensing* (48:1), 4–23.

Lowe, D. G. (2004). Distinctive image features from scale-invariant keypoints. *International journal of computer vision* (60:2), 91–110.

Lucieer, A., Jong, S. M. d., Turner, D. (2014). Mapping landslide displacements using Structure from Motion (SfM) and image correlation of multi-temporal UAV photography. *Progress in Physical Geography* (38:1), 97–116.

Mabrouk, H., Feurer, D., Massuel, S., Ben Jemaa, F. (2017). Un exemple de l'utilisation des drones dans la gestion technique d'un verger de pêcher en Tunisie. *Watch Letter* (38), 73–79.

Mantua, N. J., Hare, S. R. (2002). The Pacific Decadal Oscillation. *Journal of Oceanography* (58:1), 35–44.

Marcus, W. A., Fonstad, M. A. (2008). Optical remote mapping of rivers at sub-meter resolutions and watershed extents. *Earth Surface Processes and Landforms: The Journal of the British Geomorphological Research Group*, 33(1), 4–24.

Meager, J. J., Schlacher, T. A., Green, M. (2011). Topographic complexity and landscape temperature patterns create a dynamic habitat structure on a rocky intertidal shore. *Marine Ecology Progress Series* (428), 1–12.

Nagarajan, S., Schenk, T. (2016). Feature-based registration of historical aerial images by Area Minimization. *ISPRS Journal of Photogrammetry and Remote Sensing* (116:Supplement C), 15–23.

Newman, M., Alexander, M. A., Ault, T. R., Cobb, K. M., Deser, C., Di Lorenzo, E., Mantua, N. J., Miller, A. J., Minobe, S., Nakamura, H., Schneider, N., Vimont, D. J., Phillips, A. S., Scott, J. D., Smith, C. A. (2016). The Pacific Decadal Oscillation, Revisited," *Journal of Climate* (29:12), 4399–4427.

Parente, L., Chandler, J. H., Dixon, N. (2021). Automated Registration of SfM-MVS Multitemporal Datasets Using Terrestrial and Oblique Aerial Images. *The Photogrammetric Record*, 36(173), 12–35.

Rupnik, E., Daakir, M., Pierrot Deseilligny, M. (2017). MicMac – a free, open-source solution for photogrammetry. *Open Geospatial Data, Software and Standards* (2:1).

Salach, A. (2017). SAPC - Application for adapting scanned analogue photographs to use them in structure from motion technology. *International Archives of the Photogrammetry, Remote Sensing & Spatial Information Sciences* (42).

Sevara, C., Verhoeven, G., Doneus, M., Draganits, E. (2017). Surfaces from the Visual Past: Recovering High-Resolution Terrain Data from Historic Aerial Imagery for Multitemporal Landscape Analysis. *Journal of Archaeological Method and Theory*.

Sisson, T. W., Robinson, J. E., Swinney, D. D. (2011). Whole-edifice ice volume change A.D. 1970 to 2007/2008 at Mount Rainier, Washington, based on LiDAR surveying," *Geology* (39:7), 639–642.

Smith, M. W., Carrivick, J. L., Quincey, D.J. (2016). Structure from motion photogrammetry in physical geography. *Progress in Physical Geography* (40:2), 247–275.

Truong Giang, N., Muller, J.-M., Rupnik, E., Thom, C., Pierrot-Deseilligny, M. (2018). Second Iteration of Photogrammetric Processing to Refine Image Orientation with Improved Tie-Points. *Sensors* (18:7), 2150.

Vargo, L. J., Anderson, B. M., Horgan, H. J., Mackintosh, A. N., Lorrey, A. M., Thornton, M. (2017). Using structure from motion photogrammetry to measure past glacier changes from historic aerial photographs. *Journal of Glaciology* (63:242), 1105–1118.

Ventura, D., Bonifazi, A., Gravina, M., Belluscio, A., Ardizzone, G. (2018). Mapping and classification of ecologically sensitive marine habitats using unmanned aerial vehicle (UAV) imagery and object-based image analysis (OBIA). *Remote Sensing* (10:9), 1331.

Verhoeven, G. (2011). Taking computer vision aloft–archaeological three-dimensional reconstructions from aerial photographs with photoscan. *Archaeological prospection* (18:1), 67–73.

Vinatier, F., Arnaiz, A. G. (2018). Using high-resolution multitemporal imagery to highlight severe land management changes in Mediterranean vineyards. *Applied Geography* (90), 115–122.

Vinatier, F., Dollinger, J., Rudi, G., Feurer, D., Belaud, G., Bailly, J.-S. (2018). The Use of Photogrammetry to Construct Time Series of Vegetation Permeability to Water and Seed Transport in Agricultural Waterways. *Remote Sensing* (10:12), 2050.

Westoby, M. J., Brasington, J., Glasser, N. F., Hambrey, M. J., Reynolds, J. M. (2012). Structure-from-Motion photogrammetry: A low-cost, effective tool for geoscience applications. *Geomorphology* (179), 300–314.

Zardi, G. I., Nicastro, K. R., Porri, F., McQuaid, C. D. (2006). Sand stress as a non-determinant of habitat segregation of indigenous (Perna perna) and invasive (Mytilus galloprovincialis) mussels in South Africa. *Marine Biology* (148:5), 1031–1038.